General Disclaimer

One or more of the Following Statements may affect this Document

- This document has been reproduced from the best copy furnished by the organizational source. It is being released in the interest of making available as much information as possible.

- This document may contain data, which exceeds the sheet parameters. It was furnished in this condition by the organizational source and is the best copy available.

- This document may contain tone-on-tone or color graphs, charts and/or pictures, which have been reproduced in black and white.

- This document is paginated as submitted by the original source.

- Portions of this document are not fully legible due to the historical nature of some of the material. However, it is the best reproduction available from the original submission.

DANI MARSHALL

INFLUENCE OF COHERENT MESOSCALE STRUCTURES ON SATELLITE-BASED DOPPLER LIDAR WIND MEASUREMENTS

NASA Contract #: NAS8-35597

Monthly Progress Report

for

November 1985

Submitted by: G. D. Emmitt and S. Houston
Simpson Weather Associates, Inc.
809 E. Jefferson Street
Charlottesville, VA 22902

(804) 979-3571

A. During November we have continued our efforts to develop display routines for overlaying gridded and non-gridded data sets. The primary objective is to have the capability to review global patterns of winds and lidar samples; to zoom in on particular wind features or global areas; and to display contours of wind components and derived fields (e.g. divergence, vorticity, deformation, etc.). Figures 1 and 2 are examples of our zoom product used to evaluate a polar orbiting shuttle lidar mission. As can be seen in Figure 2, the density of cusps (i.e. locations of best wind measurements) is not very great. Ground truth for a shuttle lidar experiment may be limited to fortuitous alignment of lidar wind profiles and scheduled rawinsonde profiles. Any improvement on this would require special rawinsonde launches and/or optimization of the shuttle orbit with global wind measurement networks.

We are now able to display the ECMWF data in a variety of map projections using the NCAR graphics package. For example, the u component for the global area bounded by longitude 0^{o} and -180^{o} is contoured in Figure 3. Figure 4 is a blowup of a subarea of Figure 3 which includes the USA. The vector display of ECMWF 1000 mb winds for this subarea is provided in Figure 5a (1000 mb) and 5b (500 mb). We are now ready to overlay the lidar derived wind fields on the ECMWF fields and to produce difference fields that can be then used in follow-on model impact studies.

Because the u and v error potentials in the lidar winds are a function of distance from the orbital ground track, it is logical that there may be some peculiar patterns in the derivative fields (divergence, vorticity, etc.). Using a control wind field with a constant divergence ($du/dx = dv/dy = 10^{-5}$ sec^{-1}), the error patterns for divergence are shown in Figures 6a and 6b). The errors form a repetitive pattern but are only 10-30% of the improved divergence field values. Further evaluation of this issue used a case from AVEVAS II (see June 85 progress report). In Figures 7a-i the lidar derived fields (with and without random noise) are compared to the AVEVAS II fields. The general patterns are preserved while in detail there are some differences that could be considered significant for some applications. However, considering the potential for errors, it is encouraging to see the overall agreement.

To illustrate the dependency of the lidar winds and derivative fields upon the satellite perspective, the same AVEVAS II wind divergence field (Figure 7a) is sampled with the satellite moving along the northern boundary of the model domain (Figures 8a and 8b). Once again the general patterns are preserved while details appear to be related to the satellite perspective.

Use of the derivative fields to detect error patterns has been helpful and will become a standard method of evaluating the MPA during its development.

B. Presently, no serious contract scheduling problems are anticipated.

C. During December we expect to get our first lidar/ECMWF wind comparisons. Our goal is to provide GLAS with an error algorithm that can be used in a series of impact studies that have been discussed but not formally proposed.

Current considerations of shuttle or space station lidar experiments require us to shift our efforts from the "free-flyer" simulations to those peculiar to a low orbit, short-term proof-of-concept mission. Specifically we will focus upon:

1) the "two-pass" wind algorithm for use with the shuttle mission, and

2) determining the optimum scan angle, scan rate, and PRF for a 28.5^{o}, 500 km AGL orbit.

D.	Total cumulative costs as of 1 December 1985	$118554.26
	Total costs for reporting month of November 1985	7244.90
	Estimated costs to complete contract	$212227.00
	% of physical completion (1st and 2nd years)	56%

List of Figures

Figure 1. Doppler lidar shot pattern for the shuttle in a polar orbit.

Figure 2. Shuttle tracks and lidar shot pattern (sinusoidal) for two consecutive orbits over the U.S. The map projection is the Lambert conformal conic projection.

Figure 3. Contours of the ECMWF 500 mb East-West wind component field from the November 10, 1979, 00 GMT model run. The data extends from 180° to 0° longitude and from the south pole to the north pole (grid = 1.875°). The inner boxed area is the boundary of wind data extracted over the United States. This area is approximately 130°W to 60°W longitude and 20°N to 55°N latitude. The contour interval = 5.0 m s^{-1}; solid lines = positive u-component; dashed lines = negative u-component.

Figure 4. Contours of the subset of data of over the U.S. (see Figure 3).

Figure 5. a. Wind vectors for 1000 mb ECMWF winds over the U.S.

b. Wind vectors for 500 mb ECMWF winds over the U.S.

Figure 6. a. Divergence fields for space-based Doppler lidar estimated winds. Input wind field du/dx = dv/dy = 100 x 10^{-6} sec^{-1}. Output wind field is gridded 11 x 11 overlapping $(300\ km)^2$ areas. Contour intervals: 0.5 x 10^{-6} sec^{-1}.

b. Same as 6a, except random noise added to input wind field.

Figure 7. a. Divergence calculated for 900 mb LAMPS winds for AVEVAS II (see June 1985 report).

b. Satellite estimated divergence using 900 mb LAMPS winds.

c. Satellite estimated divergence using 900 mb LAMPS winds. Random noise is included in the input data.

d. Same as 7a except for vorticity.

e. Same as 7b except for vorticity.

f. Same as 7c except for vorticity.

g. Same as 7a except for deformation.

h. Same as 7b except for deformation.

i. Same as 7c except for deformation.

Figure 8. a. Same as 7b except satellite track is over the northern portion of the wind field.

b. Same as 7c and with satellite over the northern part of the network.

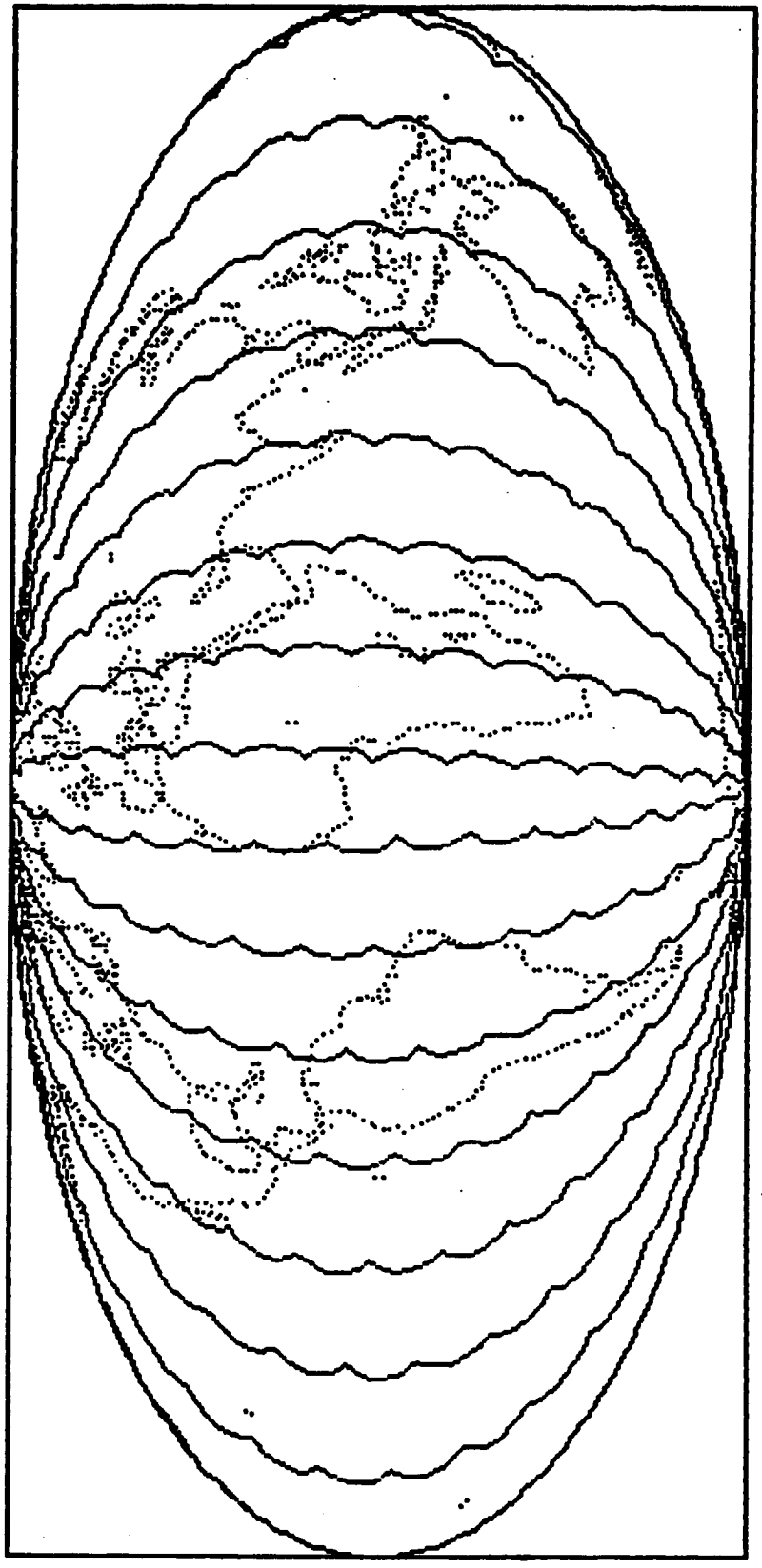

Figure 1.

SHUTTLE BASED DOPPLER LIDAR SIMULATION

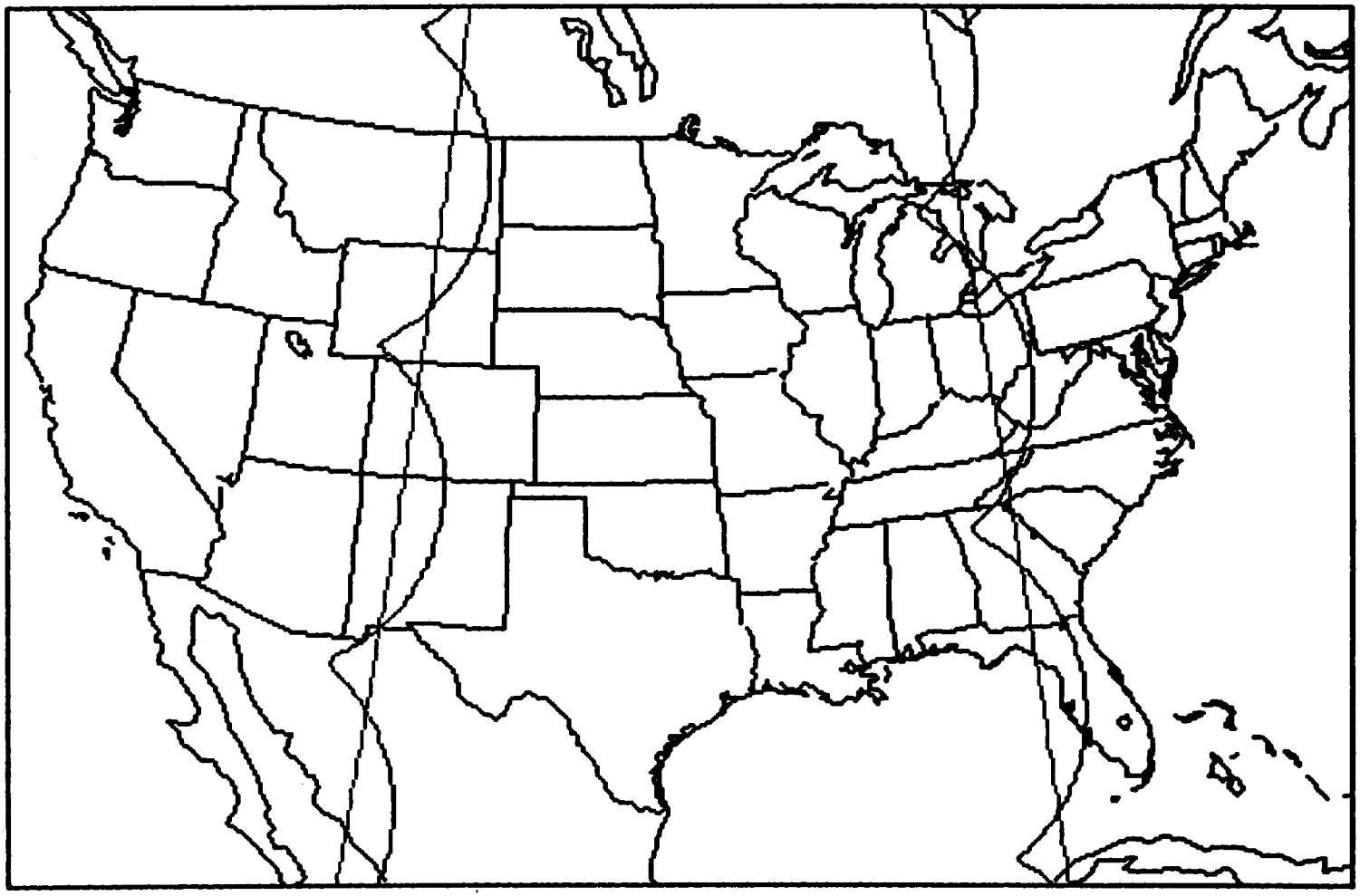

Figure 2.

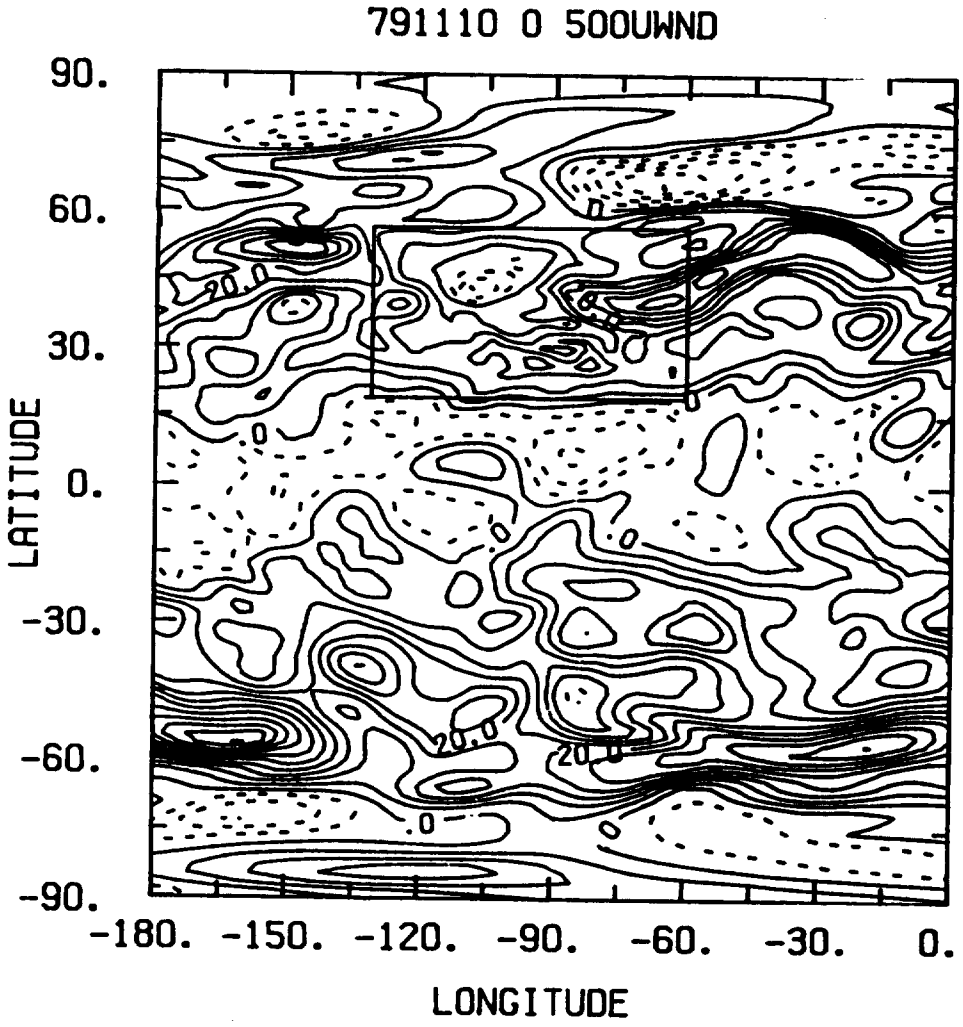
791110 0 500UWND
90.
60.
30.
0.
-30.
-60.
-90.
LATITUDE
-180.
-150.
-120.
-90.
-60.
-30.
0.
LONGITUDE
20.0
0
20.0
20.0
0
0

Figure 3.

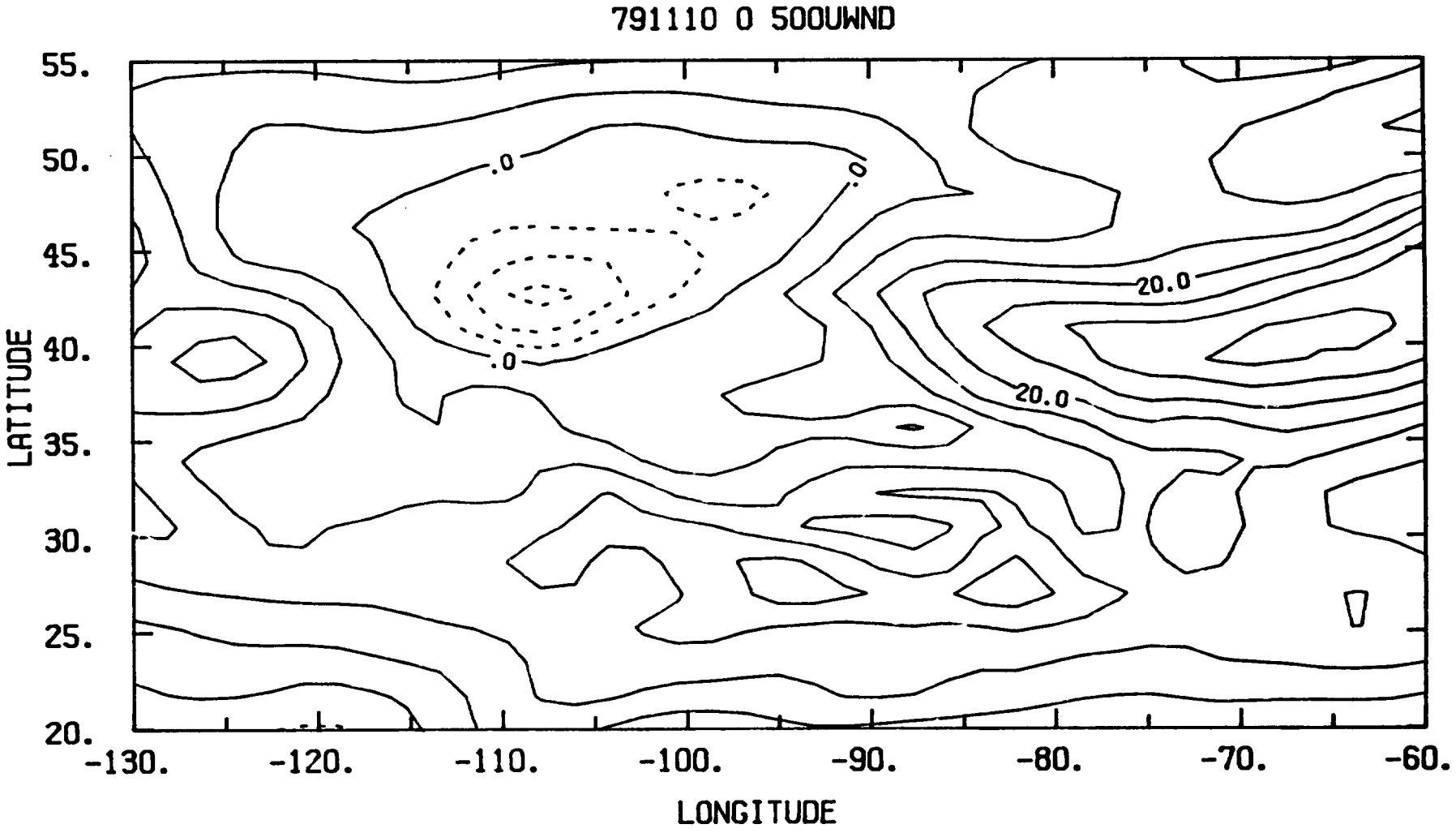
791110 0 500UWND
55.
50.
45.
40.
35.
30.
25.
20.
LATITUDE
.0
.0
.0
20.0
20.0
-130.
-120.
-110.
-100.
-90.
-80.
-70.
-60.
LONGITUDE

Figure 4.

791110 01000

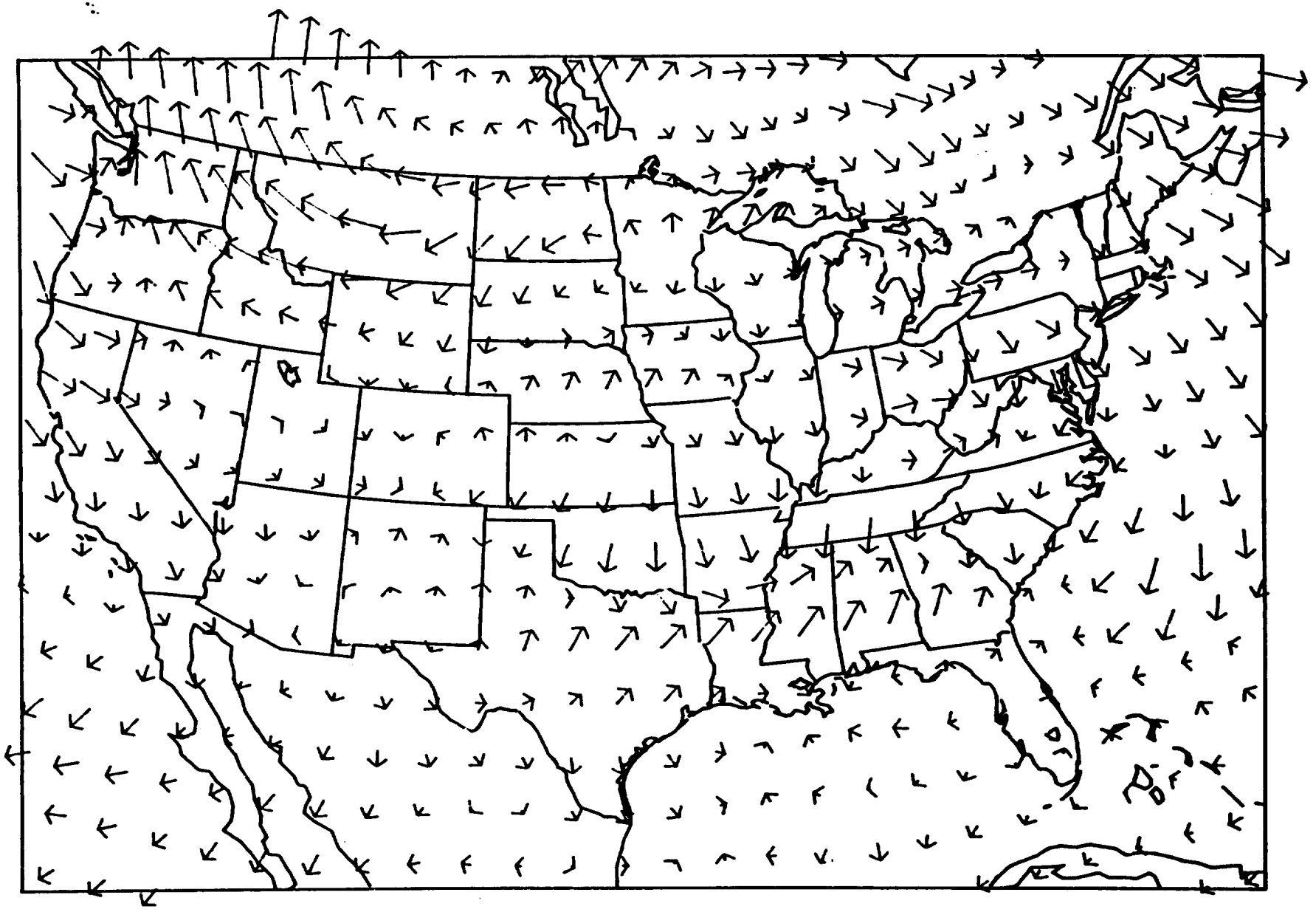

10.0 METERS PER SEC

Figure 5a.

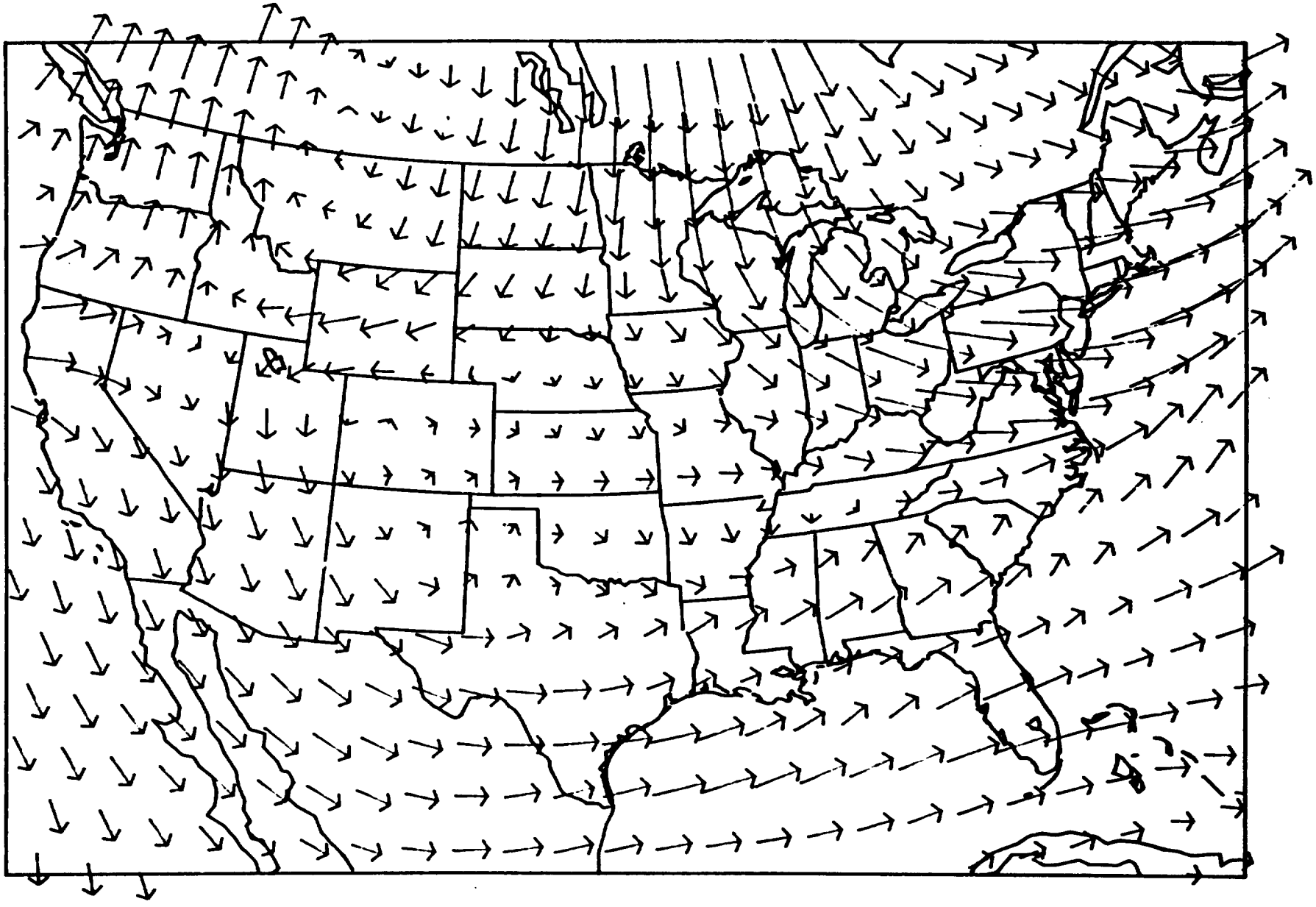

Figure 5b.

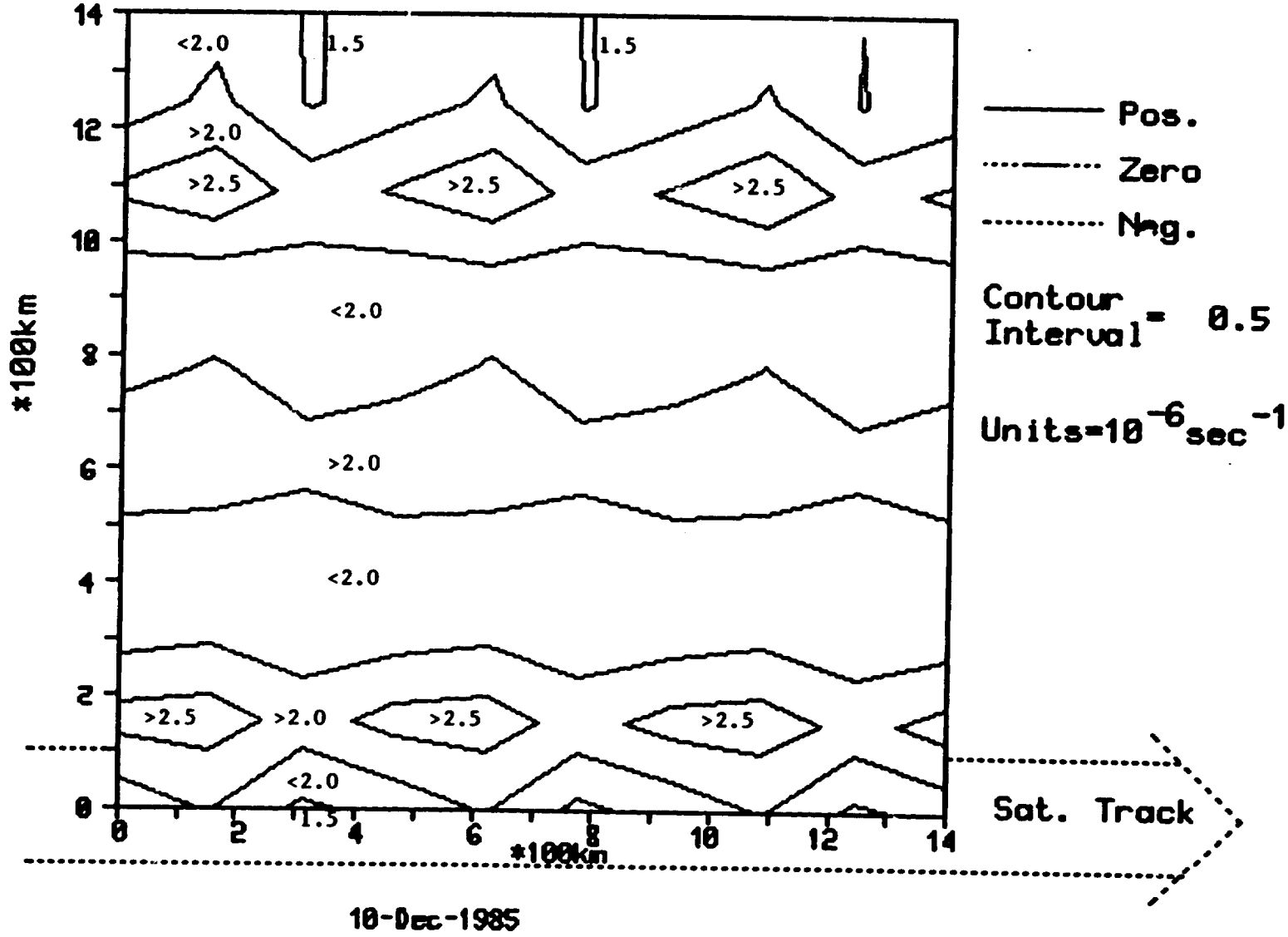
Divergence for Space-Based Doppler Lidar
Estimated Winds using Control Wind Field
*100km
*100km
<2.0
1.5
1.5
>2.0
>2.5
>2.5
>2.5
<2.0
>2.0
<2.0
>2.5
>2.0
>2.5
>2.5
<2.0
1.5
Pos.
Zero
Neg.
Contour Interval = 0.5
Units=10^-6 sec^-1
Sat. Track
10-Dec-1985

Figure 6a.

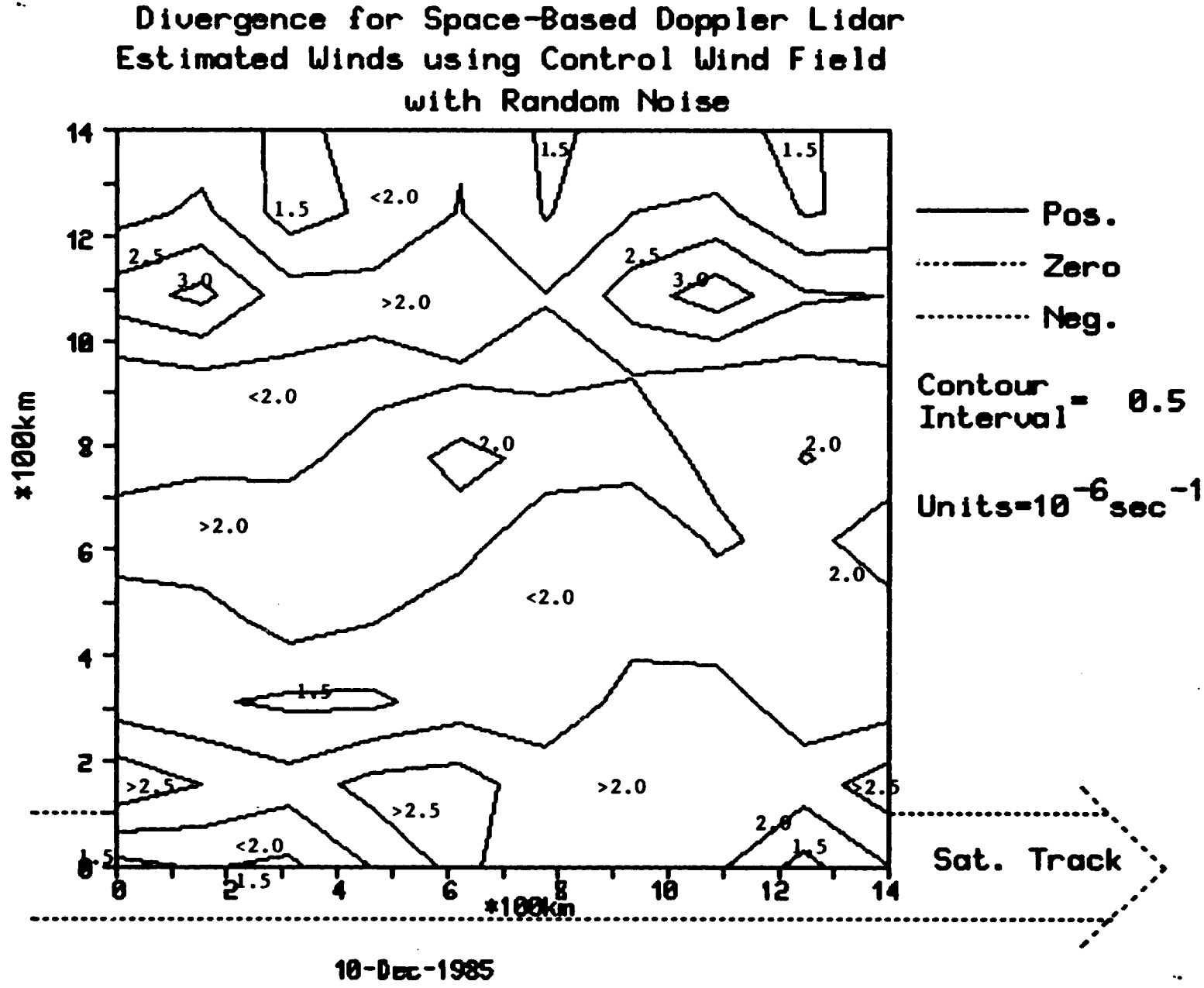
Divergence for Space-Based Doppler Lidar
Estimated Winds using Control Wind Field
with Random Noise
*100km
*100km
Pos.
Zero
Neg.
Contour Interval = 0.5
Units=10^-6 sec^-1
Sat. Track
10-Dec-1985

Figure 6b.

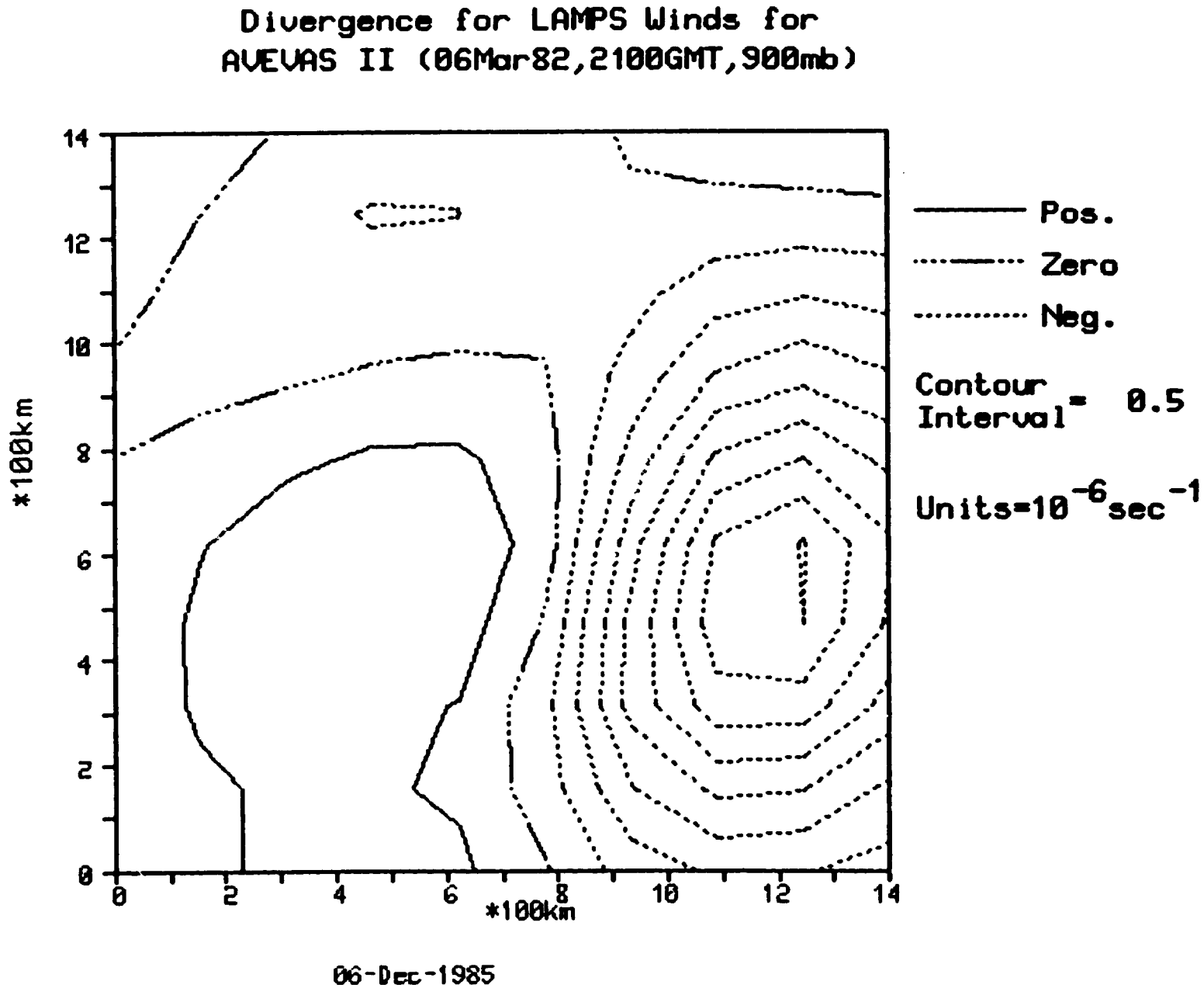
Divergence for LAMPS Winds for
AVEVAS II (06Mar82,2100GMT,900mb)
*100km
*100km
Pos.
Zero
Neg.
Contour Interval = 0.5
Units=10^-6 sec^-1
06-Dec-1985

Figure 7a.

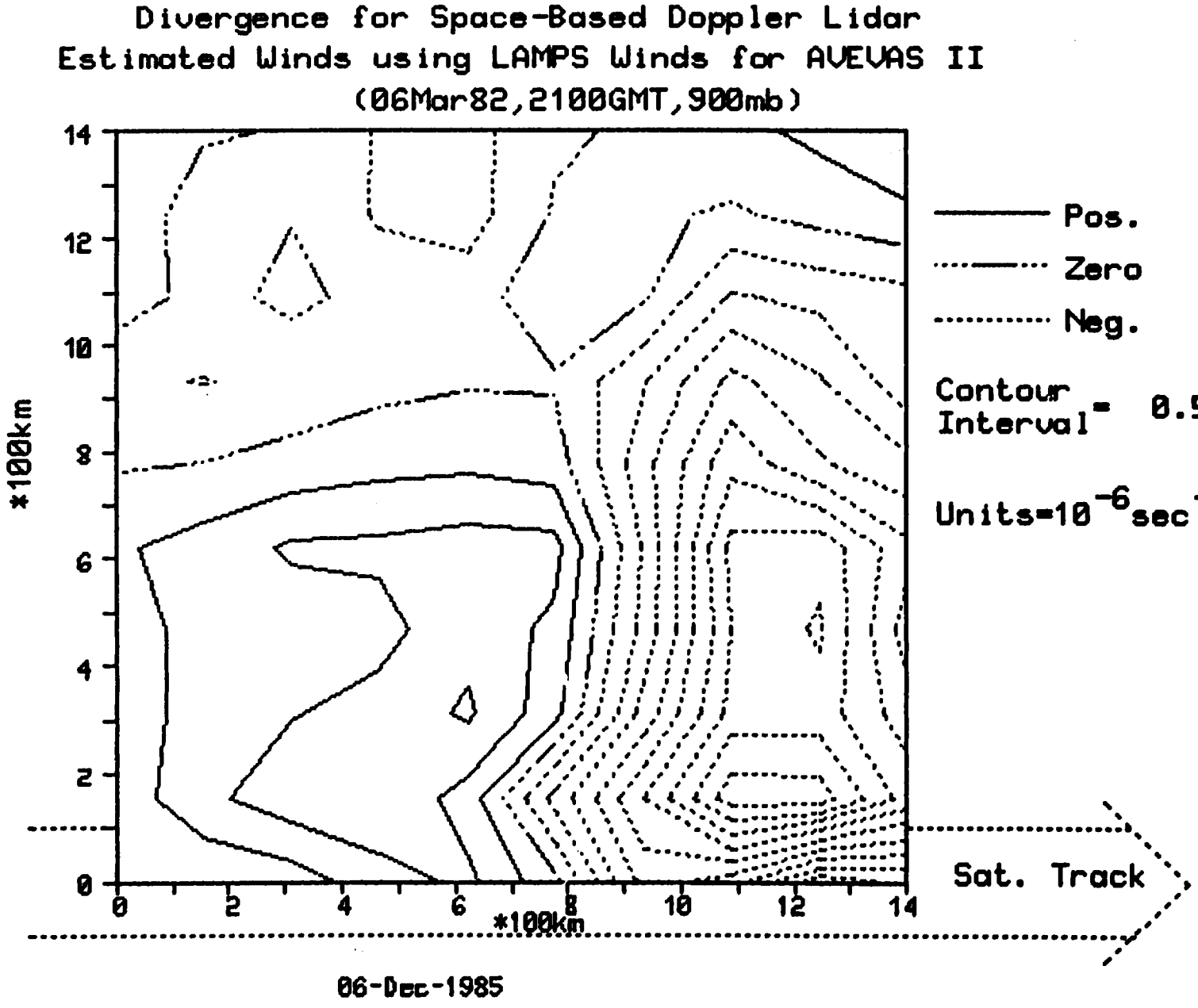
Divergence for Space-Based Doppler Lidar
Estimated Winds using LAMPS Winds for AVEVAS II
(06Mar82,2100GMT,900mb)
*100km
*100km
0
2
4
6
8
10
12
14
Pos.
Zero
Neg.
Contour Interval= 0.5
Units=10^-6 sec^-1
Sat. Track
06-Dec-1985

Figure 7b.

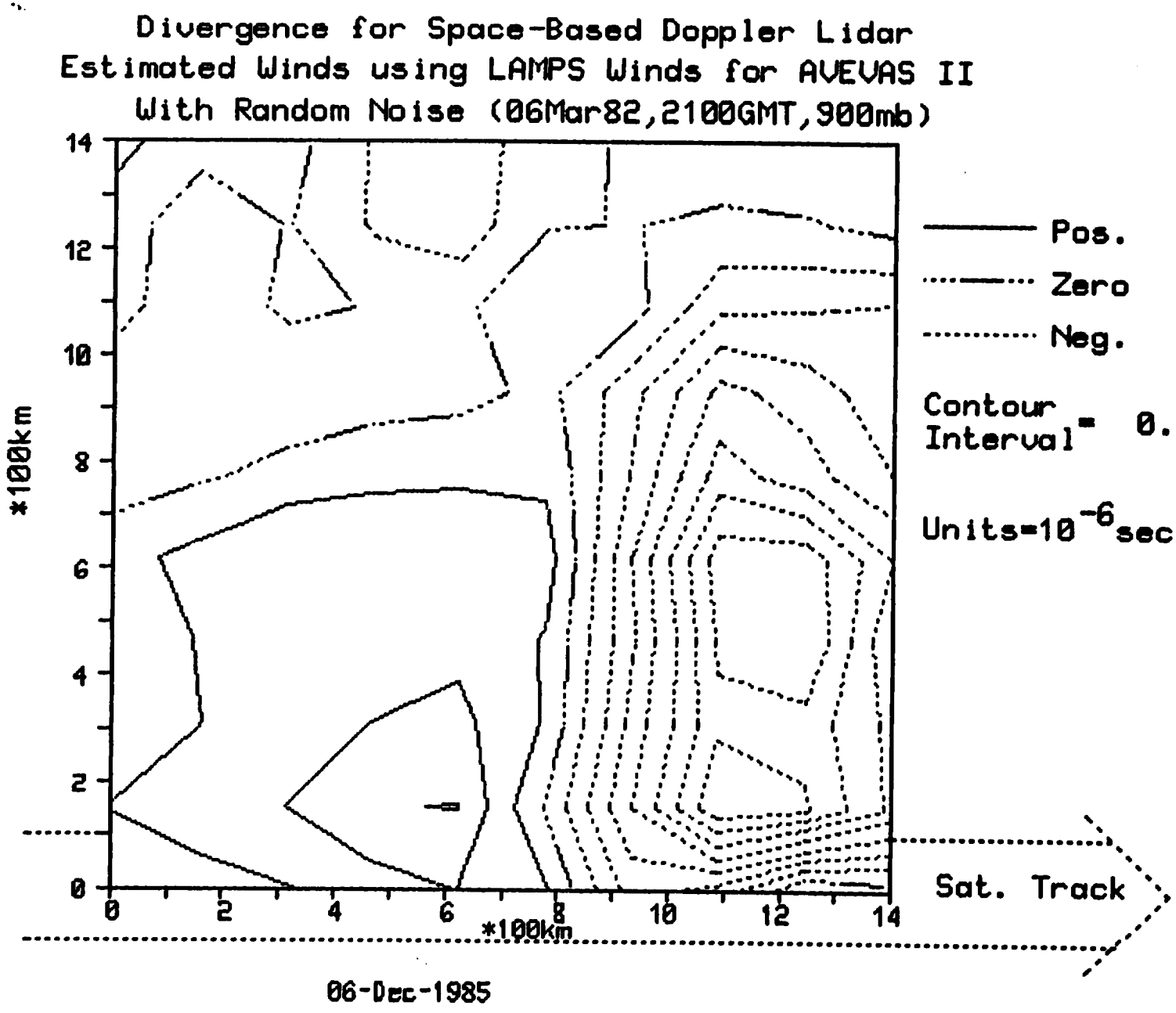
Divergence for Space-Based Doppler Lidar
Estimated Winds using LAMPS Winds for AVEVAS II
With Random Noise (06Mar82,2100GMT,900mb)
*100km
*100km
0
2
4
6
8
10
12
14
Pos.
Zero
Neg.
Contour Interval= 0.5
Units=10^-6 sec^-1
Sat. Track
06-Dec-1985

Figure 7c.

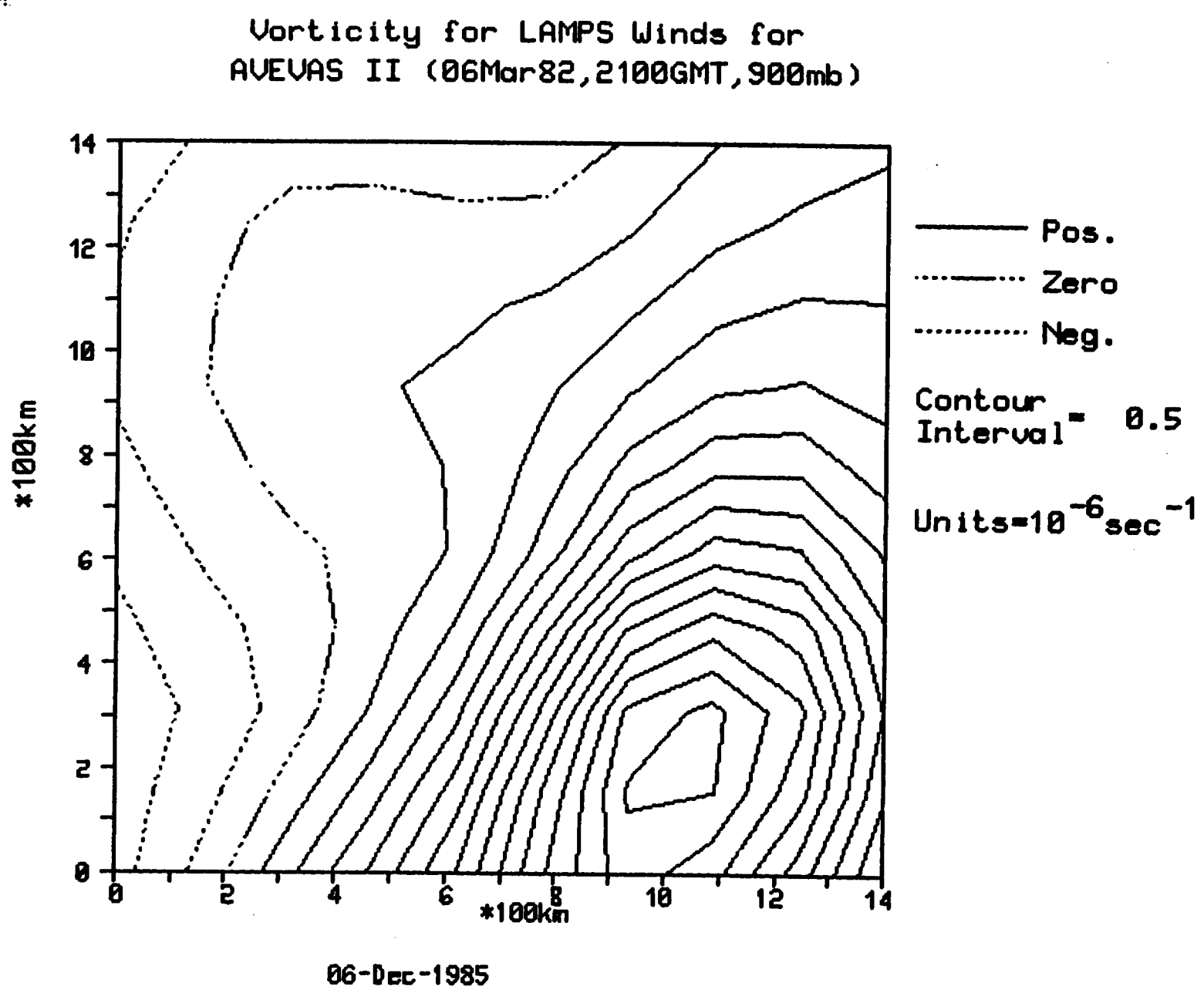
Vorticity for LAMPS Winds for
AVEVAS II (06Mar82,2100GMT,900mb)
*100km
*100km
0
2
4
6
8
10
12
14
Pos.
Zero
Neg.
Contour Interval= 0.5
Units=10^-6 sec^-1
06-Dec-1985

Figure 7d.

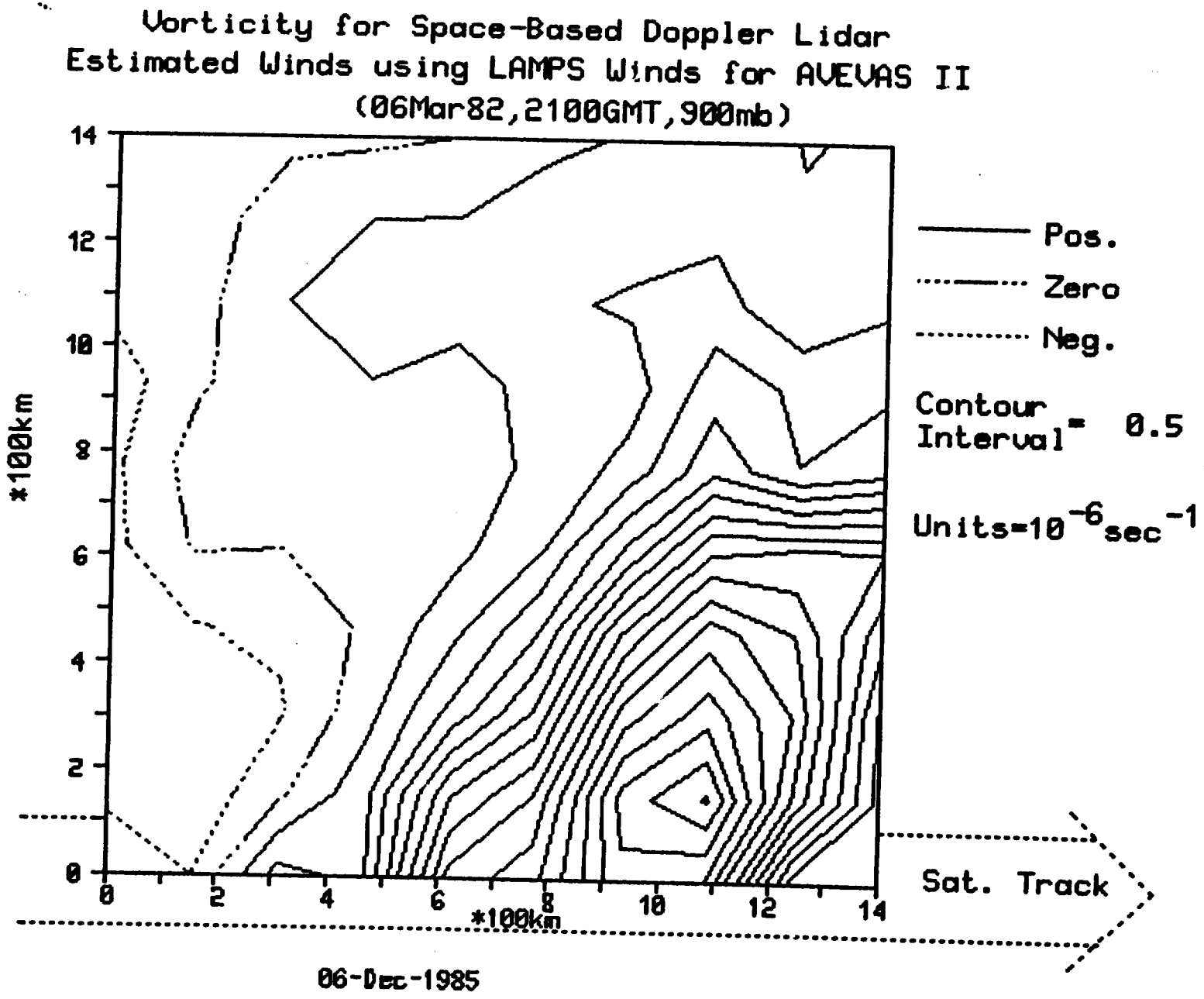
Vorticity for Space-Based Doppler Lidar
Estimated Winds using LAMPS Winds for AVEVAS II
(06Mar82,2100GMT,900mb)
*100km
*100km
0
2
4
6
8
10
12
14
Pos.
Zero
Neg.
Contour Interval= 0.5
Units=10^-6 sec^-1
Sat. Track
06-Dec-1985

Figure 7e.

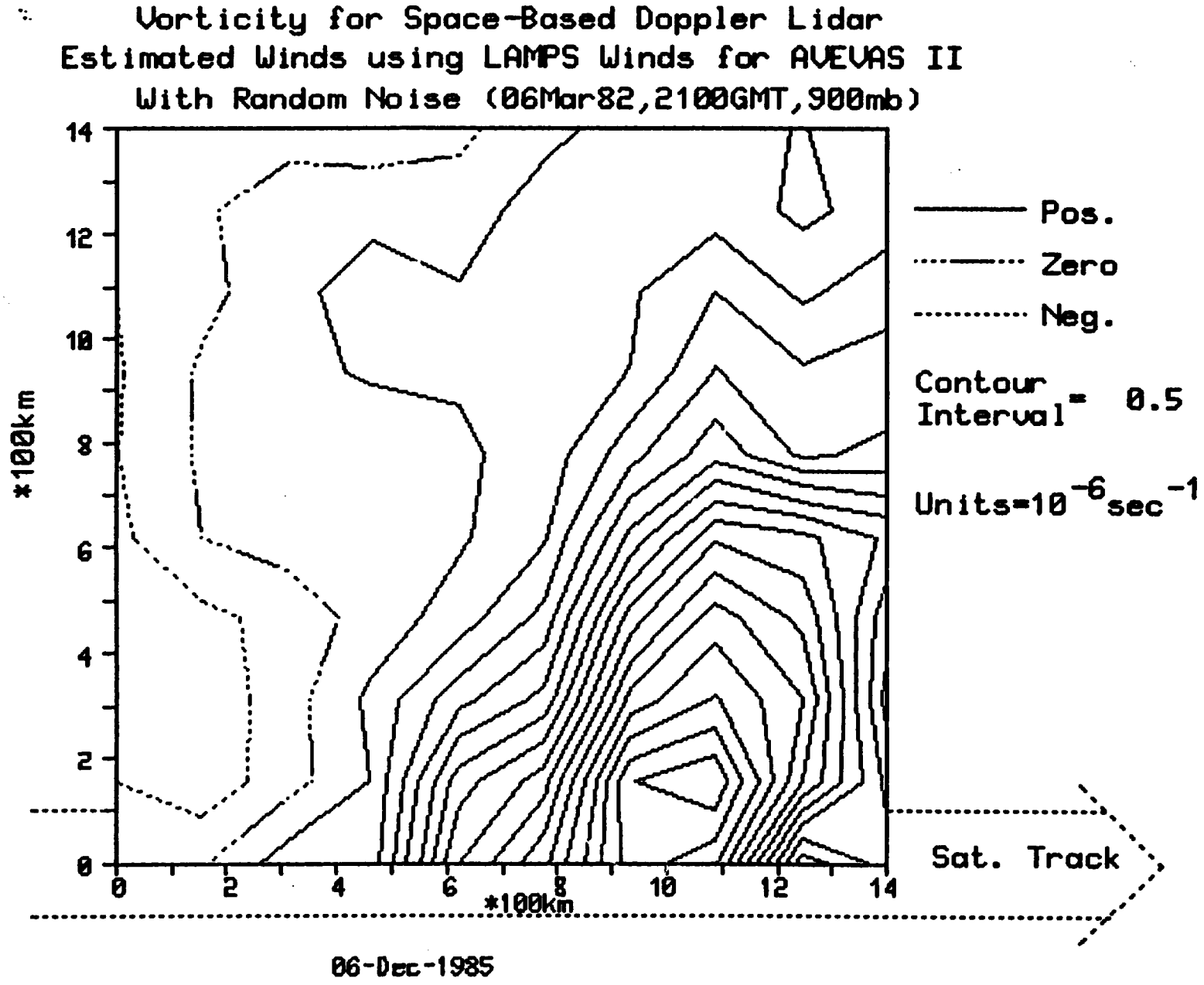
Vorticity for Space-Based Doppler Lidar
Estimated Winds using LAMPS Winds for AVEVAS II
With Random Noise (06Mar82,2100GMT,900mb)
*100km
*100km
Pos.
Zero
Neg.
Contour Interval= 0.5
Units=10^-6 sec^-1
Sat. Track
06-Dec-1985

Figure 7f.

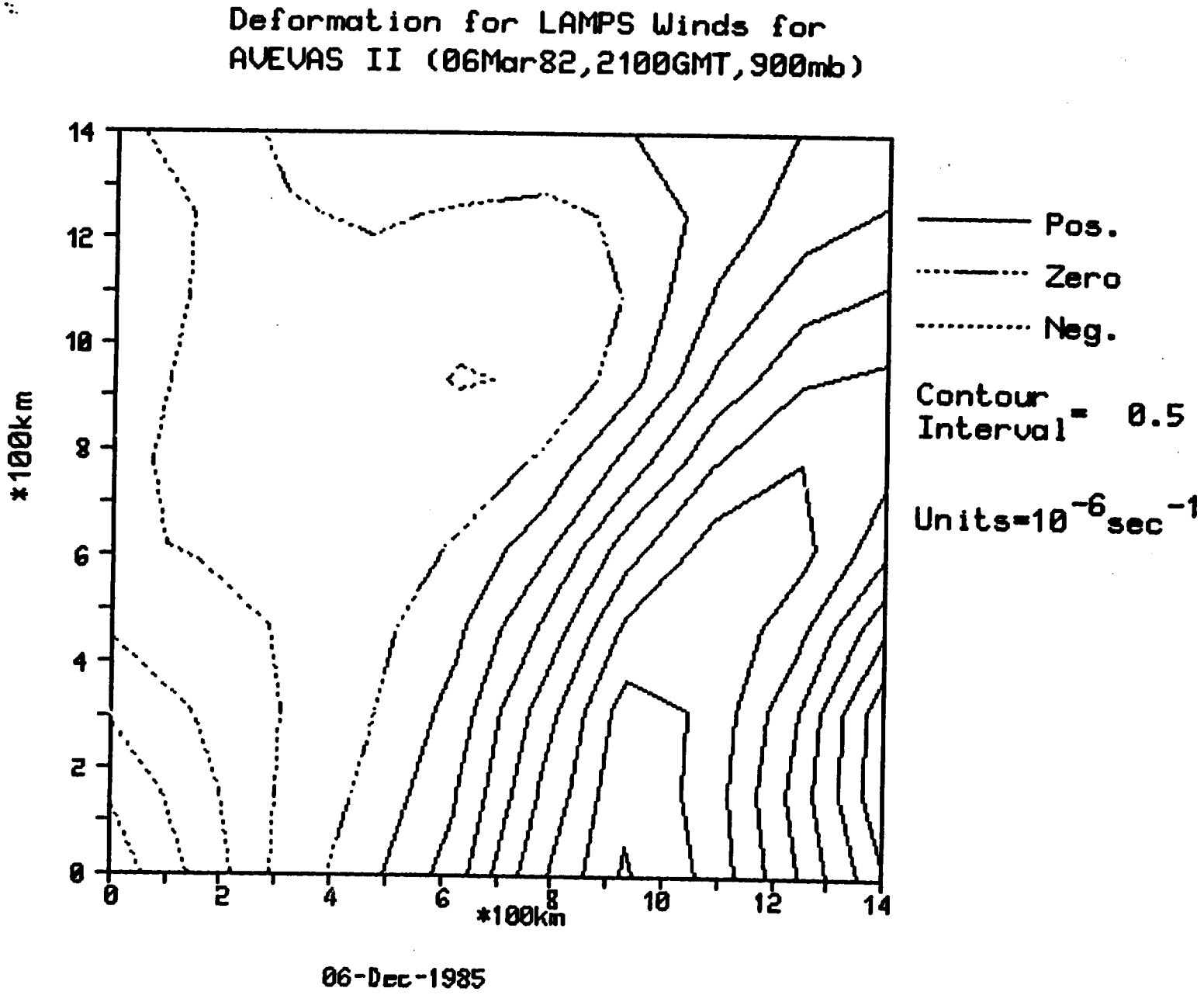
Deformation for LAMPS Winds for
AVEVAS II (06Mar82,2100GMT,900mb)
*100km
0
2
4
6
8
10
12
14
*100km
Pos.
Zero
Neg.
Contour Interval= 0.5
Units=10^-6 sec^-1
06-Dec-1985

Figure 7g.

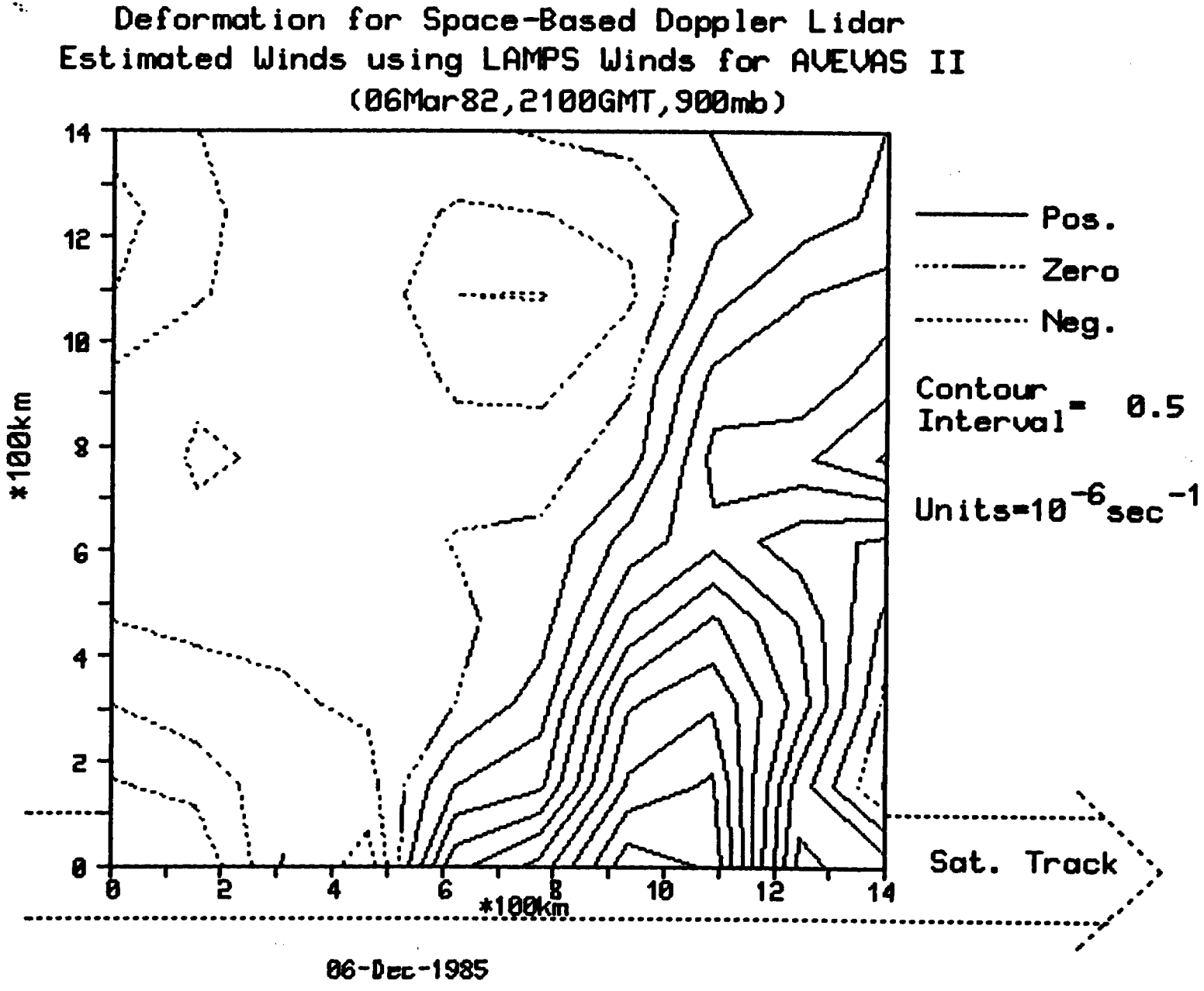
Deformation for Space-Based Doppler Lidar
Estimated Winds using LAMPS Winds for AVEVAS II
(06Mar82,2100GMT,900mb)
*100km
*100km
Pos.
Zero
Neg.
Contour Interval= 0.5
Units=10^-6 sec^-1
Sat. Track
06-Dec-1985

Figure 7h.

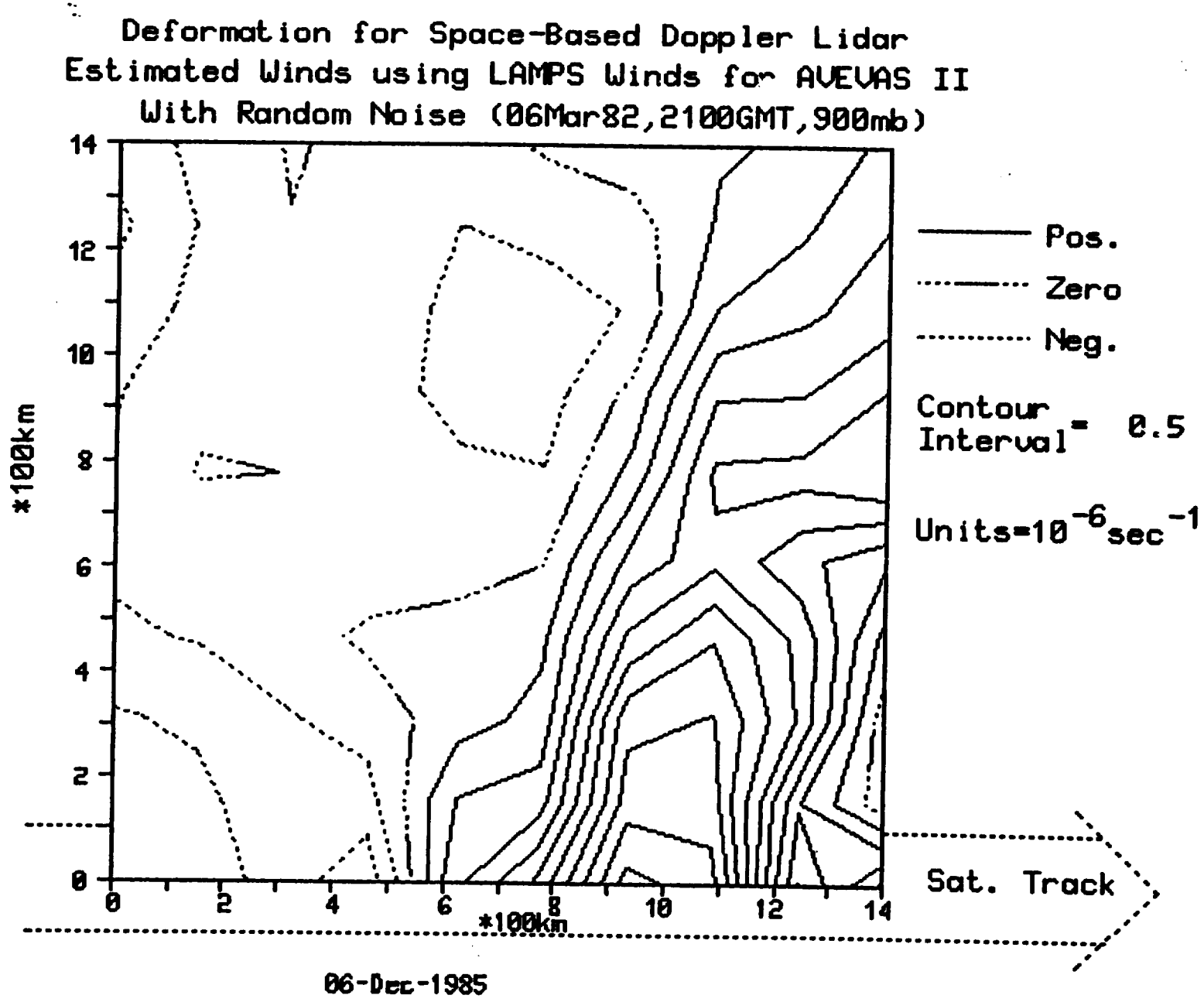
Deformation for Space-Based Doppler Lidar
Estimated Winds using LAMPS Winds for AVEVAS II
With Random Noise (06Mar82,2100GMT,900mb)
*100km
*100km
0
2
4
6
8
10
12
14
Pos.
Zero
Neg.
Contour Interval= 0.5
Units=10^-6 sec^-1
Sat. Track
06-Dec-1985

Figure 7i.

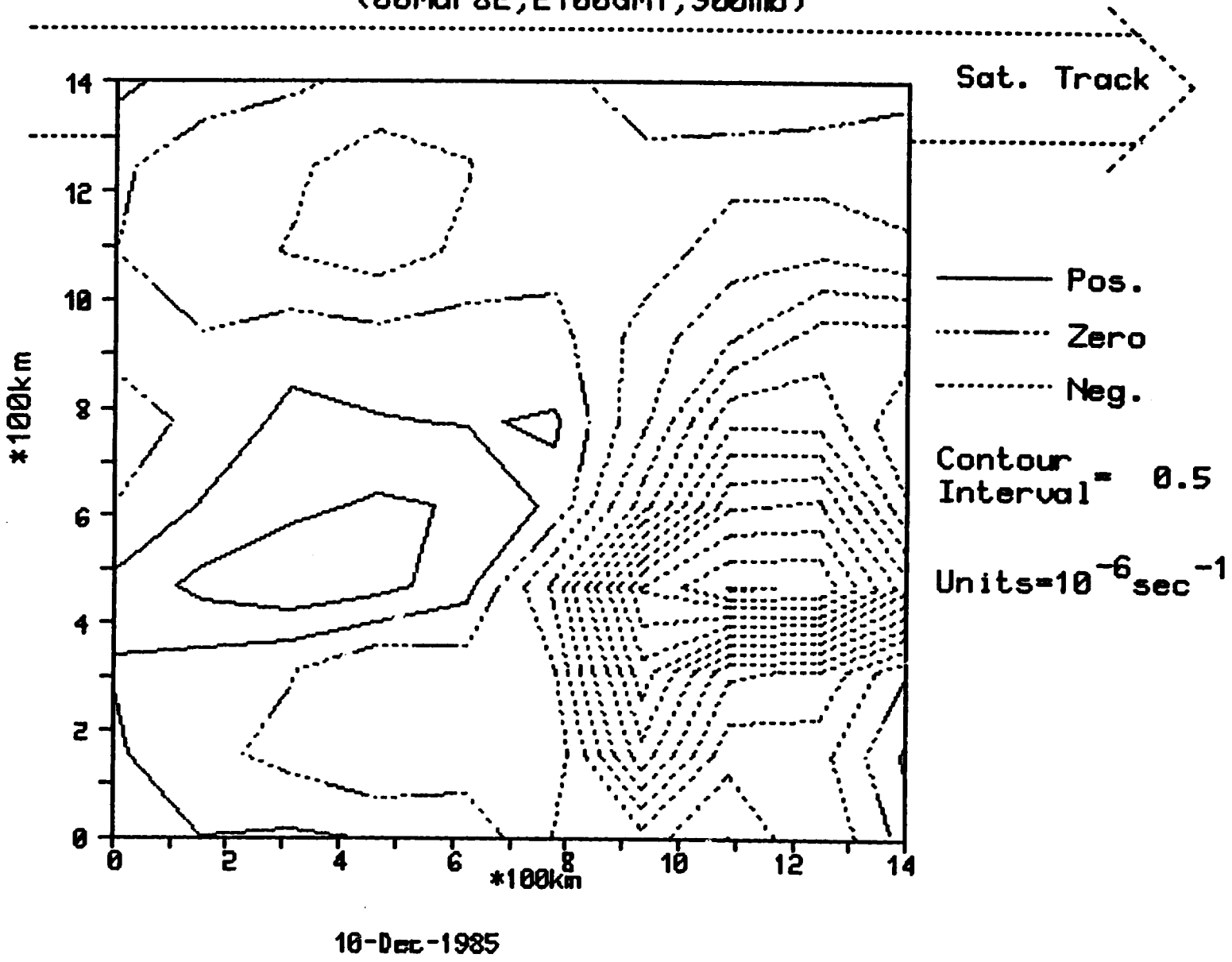
Divergence for Space-Based Doppler Lidar
Estimated Winds using LAMPS Winds for AVEVAS II
(06Mar82,2100GMT,900mb)
Sat. Track
Pos.
Zero
Neg.
Contour Interval= 0.5
Units=10^-6 sec^-1
*100km
*100km
0
2
4
6
8
10
12
14
10-Dec-1985

Figure 8a.

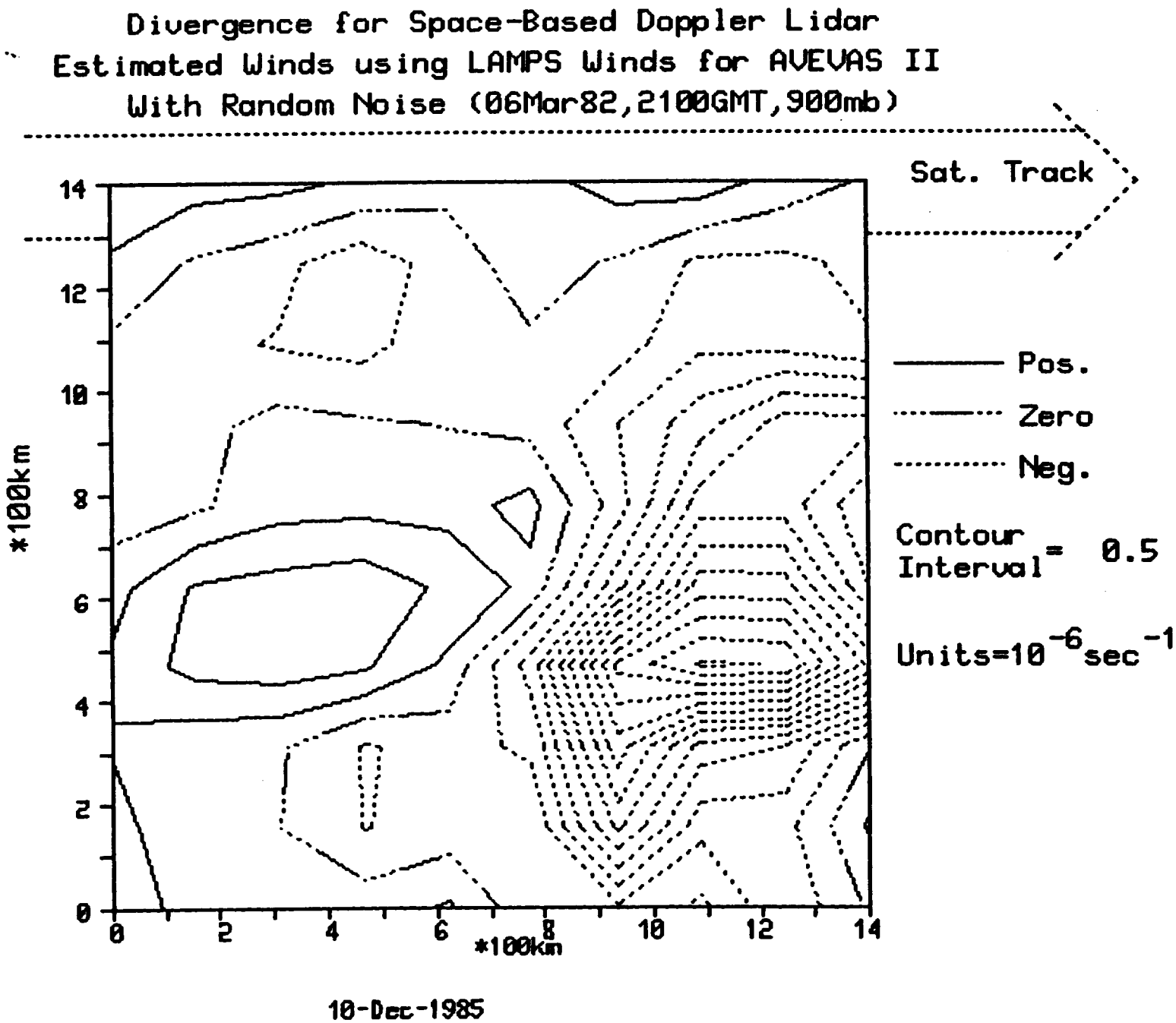
Divergence for Space-Based Doppler Lidar
Estimated Winds using LAMPS Winds for AVEVAS II
With Random Noise (06Mar82,2100GMT,900mb)
Sat. Track
Pos.
Zero
Neg.
Contour Interval = 0.5
Units=10^-6 sec^-1
*100km
*100km
0
2
4
6
8
10
12
14
10-Dec-1985

Figure 8b.